Journal of Materials Chemistry A

Improving the thermoelectric performance of TiNiSn half-Heusler via incorporating submicron lamellae eutectic of Ti70.5Fe29.5: A new strategy for enhancing the power factor and reducing the thermal conductivity

Journal:	*Journal of Materials Chemistry A*
Manuscript ID:	TA-ART-09-2014-004661.R1
Article Type:	Paper
Date Submitted by the Author:	15-Oct-2014
Complete List of Authors:	Bhardwaj, Aman; NPL-Council of Scientific and Industrial Research, CSIR-Network of Institutes for Solar Energy, MISRA, DINESH; NPL-Council of Scientific and Industrial Research, CSIR-Network of Institutes for Solar Energy

Improving the thermoelectric performance of TiNiSn half-Heusler via incorporating submicron lamellae eutectic of $Ti_{70.5}Fe_{29.5}$: A new strategy for enhancing the power factor and reducing the thermal conductivity

A. Bhardwaj and D. K. Misra*

CSIR-Network of Institutes for Solar Energy, Materials Physics & Engineering Division, CSIR-National Physical Laboratory, Dr. K. S. Krishnan Marg, New Delhi-110012.

Abstract:

The concept of composite derived by incorporating a second minor phase in bulk thermoelectric materials has established itself as an effective paradigm for optimizing the high thermoelectric performance. In this work, the incorporation of submicron lamellae eutectic phase as inclusions into cheap, abundant and non-toxic TiNiSn half-Heusler is extended for the first time to optimize its thermoelectric performance. Half-Heusler (HH) TiNiSn/eutectic $Ti_{70.5}Fe_{29.5}$ composites were fabricated employing arc-melting route followed by spark plasma sintering (SPS) technique. Incorporating metallic submicron lamellae eutectic of $Ti_{70.5}Fe_{29.5}$ into HH TiNiSn matrix results to a substantial increase in the power factor (~57% larger value than TiNiSn HH) and simultaneous reduction (~25% smaller value than TiNiSn HH) in the thermal conductivity, leading to an enhanced thermoelectric figure-of-merit (ZT) of 0.41 at 773 K for Half-Heusler (HH) TiNiSn/eutectic $Ti_{70.5}Fe_{29.5}$ composite with a mass ratio 33:1 which is 105 % higher value than the counterpart TiNiSn HH. The enhancement in power factor is primarily due to increased electrical conductivity resulted by metallic $Ti_{70.5}Fe_{29.5}$ eutectic inclusions while reduction in thermal conductivity can be ascribed to the enhanced phonon scattering by numerous lamellae interfaces of β- Ti and TiFe of eutectic phase and also their interfaces with HH phase. Effective value of thermal conductivity of HH TiNiSn/eutectic $Ti_{70.5}Fe_{29.5}$ composites calculated by the effective medium theory in the light of Maxwell–Eucken approximations, matches well with experimental value of thermal conductivity.

*Corresponding author. E-mail address: misradk@nplindia.org, dakkmisra@gmail.com (DKM)

1. Introduction

The prospects of climate change, eventual fossil fuel depletion and increasing severe CO_2 problem, has revived tremendous interest in exploring thermoelectric materials with high efficiency and thermoelectric technology. The efficiency of thermoelectric materials is gauged by dimensionless thermoelectric figure of merit $ZT = \frac{\alpha^2 \sigma T}{\kappa}$ where σ is the electrical conductivity, α, Seebeck coefficient, κ, the thermal conductivity and *T,* the absolute temperature. The figure-of-merit requires a high Seebeck coefficient α, large electric conductivity σ, and low thermal conductivity κ.[1]

In the past decades, several concepts such as phonon-glass electron-crystal, (PGEC), heavy rattling atoms as phonon absorbers, high density of states at the Fermi energy, differential temperature dependence of density of states, high effective electron mass, superlattice structures and electron-phonon coupling have been established to design the thermoelectric materials with optimized thermoelectric figure of merit. Based on these concepts, many materials such as Bi_2Te_3[2], $AgPb_mSbTe_{2+m}$ (LAST)[3], TeAgGeSb (TAGS)[4], PbTe[5], SiGe[6] Skutterudites [7] and Zintl phase compounds[8] have been widely investigated with their high ZT. Unfortunately, despite their high ZT; particularly, the state-of-the-art materials such as LAST[7] and TAGS[8] were associated with a major issue of low earth crust abundance and high market price of at least one of their components.

Among several thermoelectric materials developed so far for power generation, half-Heusler compounds (with general compositions MNiSn (n-type) and MCoSb (p-type); where M= Zr, Hf, Ti) are more environmentally benign, and hence continuously attracting tremendous interest in thermoelectric materials applications.[9] These compounds are generally semiconductors with narrow band-gap. They usually show non-parabolic band features near the Fermi level. These combined features of narrow band gap and non-parabolic band facilitate to exhibit high thermoelectric power-factor PF (=α^2 σ) and high ZT >1 in several state-of-the-art p-[10] and n-[11] type half-Heusler materials were optimized which makes them a compatible module for thermoelectric devices. However, most of these half- Heusler state-of-art materials are doped with expensive and heavy elements. In this series of materials, TiNiSn-based materials is a promising thermoelectric materials with regard to elemental abundance since they contain earth-

abundant and non-toxic elements, such as Ti and Sn.[12-14] They are easy to prepare in large scale quantities using conventional solid state synthesis. The drawback associated with these materials is extremely low value of ZT (= (PF/κ)*T) which is because of primarily, their very large thermal conductivities (κ) in comparison to the other state-of-the-art TE materials.

Many techniques such as solid solution alloying, [15-19] nanostructuring,[20] and the investigation of new structures.[21,22] have been widely employed to disrupt the heat carrying phonons in order to overcome the large thermal conductivity for increasing ZT of this class of compounds. For applications at high temperatures, where materials for power generation are needed, mostly, the majority of phonons are most effectively scattered by features on the nanoscale and therefore, significant reduction in thermal conductivities were noted, optimizing high figure of merit of several thermoelectric materials.[10(a), 11(b),11(e), 23-28]

Nanostructuring particularly the nanocomposite approach in thermoelectric has been demonstrated as an effective strategy for improving ZT by significantly reducing thermal conductivity while maintaining the electronic properties less affected or improved simultaneously. Incorporations of particles such as ZrO_2,[29-31] Al_2O_3,[32] WO_3,[33] C_{60},[34] NiO[35] and HfO_2[36] into the matrix of HH thermoelectric material have been documented very well as an efficient top-down approach to improve ZT. In such investigation, it has been attributed that the increased phonon scattering by the interface between particles and the matrix leads to significant reduction in the thermal conductivity.

Apart from such strategy of fabricating composite by incorporating of a minor phase into matrix phase, the bulk thermoelectric composites may also be derived via spontaneous partitioning of a precursor phase into thermodynamically stable phases which are also an exciting path to fabricate the composite materials.[37-43] The use of such microstructure to reduce thermal conductivity in thermoelectric materials has also been investigated.[42-44] The partitioning of quenched metastable phases into eutectic composite phases during a controlled process has also been well studied by Wu et al.[45] in order to reveal fine microstructure for enhancing the thermoelectric performance. Such eutectic composite materials have ability to rapidly prepare and even the possibility to reduce thermal conductivity.[42-45] In fact, a number of eutectic materials based on III-V and IV-VI compound semiconductors have been studied previously as

thermoelectric with high ZT due to reduced thermal conductivity. [40,43,46-51] In this direction of further reducing the thermal conductivity, metallic lamellae eutectic can be utilized as inclusion in thermoelectric matrix in order to improve the thermoelectric performance. Out of several metallic eutectic alloys, eutectic $Ti_{70.5}Fe_{29.5}$ is a low cost potential lightweight engineering materials for industrial applications due to their excellent mechanical properties with yield strength ~1000 MPa, fracture strength (~2000–2600 MPa) and larger plasticity (>2%).[52,53] Moreover, incorporation of such metallic inclusion can increase the carrier concentration which may increase the electrical conductivity and partially aligned lamellae of β-Ti and TiFe interfaces may enhance the additional phonon scattering for further for reducing the thermal conductivity of these composite.

Herein we appeal the aspect of such submicron lamellae structure of eutectic phase to be incorporated in the existing potential thermoelectric matrix to improve ZT. We believe that it is highly possible that metallic submicron lammmellae eutectic inclusions will lead to reduced κ due to numerous interfaces for phonon scattering together with large σ due to metallic inclusions which perhaps will further improve the thermoelectric properties. To the best of our knowledge the incorporation of eutectic phase inclusions into thermoelectric materials has seldom been reported so far to see its effect on the thermoelectric properties. In this work, we investigate the effect of metallic eutectic inclusions in cheap, non toxic and environmentally friendly and potential thermoelectric matrix of HH TiNiSn on the thermoelectric properties. The electrically conductive eutectic $Ti_{70.5}Fe_{29.5}$ which is highly stable, was prepared by arc melting method described in our previous report.[53,54] A reduced κ was realized due to the enhanced phonon scattering by numerous submicron lamellae interfaces of β- Ti and TiFe eutectic phases and grain boundaries. In conjunction with reduction in thermal conductivity, the power factor is also increased due to enhanced electrical conductivity, leading to the improvement of ZT of 0.41 at 773K for Half-Heusler (HH) TiNiSn/eutectic $Ti_{70.5}Fe_{29.5}$ composite with a mass ratio of 33:1.

2.0 Experimental Details:

2.1 Materials Processing

TiNiSn (HH) and $Ti_{70.5}Fe_{29.5}$ were synthesized by direct arc-melting of Titanium (Ti; 99.99%, Alfa Aesar, powder), nickel (Ni; 99.99%, Alfa Aesar, powder), tin (Sn; 99.99%, Alfa Aesar

powder) and Iron (Fe; 99.99%, Alfa Aesar, powder) in stoichiometric composition of TiNiSn and $Ti_{70.5}Fe_{29.5}$. For synthesis of TiNiSn compound, the Sn was kept on the top above Ti and Ni which was initially melted and then molten Sn diffuses into (Ti and Ni) matrix. The resulted TiNiSn melted ingot was then annealed at 1073K for one week under vacuum in a quartz tube which helps to accelerate atomic diffusion throughout the matrix for stabilization of phases to get a homogeneous phase. The both ingots were then subsequently broken into small pieces and grounded to a very fine powder by using mortar and pestil. The powder of TiNiSn half-Heusler and powder of eutectic $Ti_{70.5}Fe_{29.5}$ were mixed together in different mass ratios of 100:1, 33:1 and 20:1 employing planetary high energy ball milling to obtained homogeneous and well-distributed mixture. These mixtures were consolidated employing spark plasma sintering (SPS) at temperatures of 1073K and pressure of 50 MPa for holding time of 10 minutes using graphite die of 12.7 mm diameter to get 12.7 mm diameter bulk dense pellets. The obtained samples were cut into two pieces, one is in the form of bar about $3 \times 2 \times 10$ mm^3 and another one is 12.7 mm diameter discs which were used for measuring the electronic and thermal transport.

2.2 Powder X-ray Diffraction

The gross structural characterization of Half-Heusler (HH) TiNiSn/eutectic $Ti_{70.5}Fe_{29.5}$ composites were carried out by powder X-ray diffractometer (Rigaku Mini Flex II) in reflection θ- 2θ geometry, with position sensitive detector (Ultafast D Tex), operating at 30 kV and 20 mA, using a graphite monochromator and CuK_{α} radiation with wavelength $\lambda \approx 1.5406$Å along with $CuK_{\alpha 2}$ filter and rotating anode equipped with powder 2θ diffractometer ranging from 20 to 80 degrees. The experimental conditions and parameters such as sample size, power ratings of X-ray tube (30kV, 20 mA) and other diffractometer parameters such as scan speed, counting steps etc. were kept constant for all diffraction experiments.

2.3 Electron microscopy

The microstructure investigation of host TiNiSn HH compound and HH TiNiSn/eutectic $Ti_{70.5}Fe_{29.5}$ composite with mass ratio 33:1 was carried out by field emission scanning electron microscopy (FE-SEM; Model: SUPRA40 VP, operating at 30kV) and HRTEM (Modell: Technai G^2F^{30};STWIN) operating at 300kV. The TEM specimens were prepared in three steps. Initially, the SPS processed pellets were cut into 3 mm discs using an ultrasonic disc cutter (Model: Gaton

170). The specimen was then mechanically polished with a load of 15 g using a dimple grinder (Model: South Bay Technology 515) and finally an electron transparent specimen for TEM analysis was achieved by Ar+-ion milling (Model: Boltech RES 101). The elemental analysis of the samples was performed using energy dispersive spectroscopy (EDS) attached to the FE-SEM.

2.4 Thermoelectric Properties

Thermal diffusivity of HH TiNiSn/eutectic $Ti_{70.5}Fe_{29.5}$ composites (with mass ratios of HH: $Ti_{70.5}Fe_{29.5}$ to 100:1, 33:1, 20:1) samples were measured by using a laser flash system (Linseis, LFA 1000) on disk-shaped specimens with approximate thickness of 2.0 mm and diameter of 12.7 mm. The disc specimens used for thermal diffusivity were sprayed with a layer of graphite in order to minimize errors due to emissivity. Specific heat was determined by a Differential scanning calorimetry (DSC) instrument (822e Mettler Toledo). The thermal conductivity of composites was calculated using the relation, $\kappa = d \times Cp \times \rho$ where d is the thermal diffusivity, ρ the geometrical pellet density and Cp the heat capacity. The Seebeck coefficient and resistivity were measured simultaneously employing commercial equipment (ULVAC, ZEM3) over the temperature range of 300 K to 773 K on samples of polished bars of about $3 \times 2 \times 10$ mm^3.

3.0 Results and Discussion

3.1 X- ray Diffraction Analysis:

The power XRD patterns of TiNiSn, $Ti_{70.5}Fe_{29.5}$ and HH TiNiSn/eutectic $Ti_{70.5}Fe_{29.5}$ composite with mass ratio of 33:1 are shown in the fig. 1a & b. The XRD patterns were indexed and the cell constants were refined by the POLSQ FORTRAN program.[55] Fig 1(a) shows XRD pattern of TiNiSn HH sample. All the peaks in XRD pattern (fig. 1a) are well indexed with cubic crystal system (space group $F\bar{4}3m$; no. 216) based on JCPDS card (No # 00-023-1281). It can be noted that usually unreacted elements and intermetallic compounds have been noted to be precipitated by several reports due to incongruent melting of TiNiSn system.[28,58,60] However, we are not able to detect such impurities in the background of XRD and electron microscopy investigations. The absence of such impurities could be due to enough precaution paid during synthesis procedure combined with arc-melting and long time annealing as described in the experimental details. The

lattice parameter was computed to be 0.594 ± 0.513x10^{-4} nm using POLSQ FORTRAN program.[88] The unit cell of TiNiSn is shown in the inset of Fig. 1(a). Fig. 1(b) presents the XRD pattern of $Ti_{70.5}Fe_{29.5}$ eutectic phase and HH TiNiSn/eutectic $Ti_{70.5}Fe_{29.5}$ composite with mass ratio of 33:1. All the peaks observed for $Ti_{70.5}Fe_{29.5}$ are well matched with β-Ti (space group $Im\bar{3}m$; no. 229) phase and the TiFe (space group Pm3m; no. 221) phase of $Ti_{70.5}Fe_{29.5}$ eutectic alloy. The lattice parameter of the β-Ti solid solution, a=0.318 ± 0.513x10^{-4} nm in $Ti_{70.5}Fe_{29.5}$ alloy was considerably smaller than that of pure β-Ti (0.3307 nm) owing to the dissolution of Fe while the lattice parameter of the TiFe phase was 0.299± 0.614x10^{-4} nm in $Ti_{70.5}Fe_{29.5}$ alloy which was larger than that for the equiatomic FeTi phase (0.2975 nm) owing to the dissolution of Ti similar to our earlier report.[53,54] The standard patterns for pure β-Ti and TiFe phase reflections are also shown in Fig. 1(b) to compare the observed XRD patterns. The XRD pattern of HH TiNiSn/eutectic $Ti_{70.5}Fe_{29.5}$ composite with mass ratio of 33:1(Fig 1b) reveals the major prominent peaks corresponding to only HH and no evident peaks corresponding to β-Ti and TiFe phases of $Ti_{70.5}Fe_{29.5}$ eutectic alloy were noticed which could be due to small amount of eutectic $Ti_{70.5}Fe_{29.5}$ inclusions to strongly diffracted x-ray radiation.

3.2 Scanning and Transmission Electron Microscopy:

In order to further identify the phases and microstructural details, the SEM and TEM of TiNiSn, $Ti_{70.5}Fe_{29.5}$ and HH TiNiSn/eutectic $Ti_{70.5}Fe_{29.5}$ composite with mass ratio of 33:1 have been performed. The SEM morphology taken corresponding to TiNiSn sample clearly reveals a single phase contrast as shown in Fig. 2a. The EDAX analysis (Fig 2b) confirms this sample as a pure TiNiSn half-Heusler phase which is also consistent with the XRD analysis. Figure 2(c) presents SEM morphology obtained from the sample of eutectic $Ti_{70.5}Fe_{29.5}$ alloy displaying alternating bright and dark phases comprising typical eutectic microstructure feature. These lamellae are confirmed as β-Ti (A2) and FeTi (B2) by EDAX analysis as marked in Fig 2(d). Interestingly, one can observe that the eutectic colonies grow (Fig. 2d) by forming sharp eutectic cell boundaries similar to our earlier report.[53] The eutectic spacing was observed to be in range of 600 to 1200 nm. The widths of β-Ti (A2) and FeTi (B2) lamellae eutectic were noted to be in the range of 400nm to 800 nm and 300 nm to 700 nm respectively showing submicron level feature of lamellae eutectic. Fig 2 (e) shows the SEM morphology of HH TiNiSn/eutectic

$Ti_{70.5}Fe_{29.5}$ composite with mass ratio of 33:1 revealing the two phase mixture. For better resolution of eutectic feature in the composite sample, the Fig 2(e) was further magnified and a clear lamellae eutectic feature can be envisaged as shown in Fig 2f. The exact composition of the eutectic is confirmed by EDAX analysis which is presented in Fig. 2(f).

Transmission electron microscopy of TiNiSn HH and HH TiNiSn/eutectic $Ti_{70.5}Fe_{29.5}$ composite with mass ratio of 33:1 has been carried out to see the microstructure and their internal structure. Fig. 3(a) displays bright field electron micrograph corresponding to TiNiSn HH showing grains with sizes ranging from 0.1 μm to 8 μm. The selected area electron diffraction (SAED) corresponding to one of the grains presents HH phase with zone axis $[1\bar{1}1]$. The bright field TEM image of TiNiSn HH/ $Ti_{70.5}Fe_{29.5}$ eutectic composite with mass ratio of 33:1 is presented in Fig 3(c) showing two phase contrasts, one with eutectic feature (marked be dotted area) and HH as matrix phase. The relatively better clarity of the eutectic feature is presented in the inset of Fig. 3(c). The SAED pattern taken from the eutectic feature as shown in Fig 3(d) confirms it to be β-Ti and TiFe of eutectic phase. In spite of looking the nature of grain boundaries interface in TEM image at HRTEM mode, we could not discern atomic scale resolution features of grain boundaries interface either due to thick samples or due to lesser instrumental resolution to detect such minor features.

3.3 Electronic and thermal transport properties:

The electronic and thermal transport properties of all the composites have been compared with the parent TiNiSn (HH) material. Figure 4(a) shows the temperature dependence of electrical conductivity (σ), of HH TiNiSn/eutectic $Ti_{70.5}Fe_{29.5}$ composites for different mass ratios. Regardless of the temperature, the electrical conductivity increases with increasing $Ti_{70.5}Fe_{29.5}$ eutectic phase concentration and reaches its maximum value for the composite with mass ratio 20:1. With rising temperature, the σ (T) also increases for all the composite samples. However, the temperature dependent behavior is not strongly dominating, showing that the composites are highly doped degenerate semiconducting materials. The room temperature measurements of the Hall coefficient (R_H) were used to determine a Hall carrier concentration ($n= 1/R_H e$) for all composites. Interestingly, the carrier concentration at room temperature increases with increasing concentration of metallic $Ti_{70.5}Fe_{29.5}$ eutectic phase. Further, the room

temperature electrical conductivity, and carrier concentration n are used to calculate the room temperature mobility (μ) by a relation $\sigma = ne\mu$ (where n is the carrier concentration, e is the charge of an electron and μ is the carrier mobility) and results are shown in table 1. In the light of room temperature Hall data, we may infer that the increased electrical conductivity of HH TiNiSn/eutectic $Ti_{70.5}Fe_{29.5}$ composites are ascribed to the increase of carrier concentration induced by incorporating metallic $Ti_{70.5}Fe_{29.5}$ eutectic in the HH matrix. We also noticed that the electron mobility of composites increases with increasing metallic inclusions. We, therefore, reasonably believe that the partially aligned lamellae of β-Ti and TiFe of $Ti_{70.5}Fe_{29.5}$ eutectic phase are most likely to provide a continuous electronic transport path as evidenced by high electron mobility which gives a higher electrical conductivity.

The temperature dependent Seebeck coefficients for bare TiNiSn (HH) and HH TiNiSn/eutectic $Ti_{70.5}Fe_{29.5}$ composites are shown in Fig 4(b). The Seebeck coefficients of all the samples are large and negative indicating that electrons are the majority carriers in these samples (n-type). Interestingly, the associated decrease in the Seebeck coefficients observed for all the composites at room temperature is consistent with increased electrical conductivity. This phenomenon of inverse relation between α and σ can be explained by the equation,56

$$\alpha = \pm\frac{k_B}{e}\left[2 + ln\frac{2(2\pi m^* k_B T)^{\frac{3}{2}}}{h^3 n}\right] \quad \text{.....(1)}$$

Where m* is the effective mass relating the density of states and n, the carrier concentration. As noted above, the introduction of metallic $Ti_{70.5}Fe_{29.5}$ eutectic phase induces large carrier concentration and hence according to the equation, α is reduced.

The temperature dependent Seebeck coefficient of all the composite samples increases with temperature up to 773 K similar to increase in the electrical conductivity with rising temperature. Usually in semiconductor, the simultaneous increase in σ and α is not expected and would require a high temperature Hall measurement to have better understanding.

Figure 4(c) displays the power factor (PF=$\alpha^2\sigma$) of matrix TiNiSn (HH) and HH TiNiSn/eutectic $Ti_{70.5}Fe_{29.5}$ composites. Interestingly, all the composites except HH

TiNiSn/eutectic $Ti_{70.5}Fe_{29.5}$ composite with mass ratio 20:1 exhibit higher power factor compared to matrix TiNiSn (HH) which is mainly ascribed to the increased σ. We noticed a small decrease in α and that is compensated by this large increase in σ to achieve their large power factor. The highest power factor of 18.05 x 10^{-4} W/mK^2 at 773K was optimized for the HH TiNiSn/eutectic $Ti_{70.5}Fe_{29.5}$ composite with mass ratio of 33:1 which is ~57% larger than the bare TiNiSn (PF= 11.43 x 10^{-4} W/mK^2).

Figure 5(a) displays the temperature dependence of total thermal conductivity κ (T) of bare TiNiSn (HH) and HH TiNiSn/eutectic $Ti_{70.5}Fe_{29.5}$ composites. Regardless to the temperature, the total thermal conductivity decreases with increasing concentration of metallic submicron lamellae eutectic $Ti_{70.5}Fe_{29.5}$ phase in the TiNiSn (HH) thermoelectric matrix. With increasing temperature, the total thermal conductivity, κ also decreases indicating that phonon conductivity dominates. Interestingly, the TiNiSn HH/ $Ti_{70.5}Fe_{29.5}$ composites with mass ratio 33:1 displayed a low thermal conductivity (~ 3.42 W/mK) at 773 K which is 25% lower than the bare TiNiSn. The reduction in thermal conductivity can be ascribed by the enhanced phonon scattering by numerous submicron lamellae interfaces of β-Ti and TiFe eutectic phase and also by grain boundaries. We attribute that the incorporation of submicron lamellae of β-Ti and TiFe of $Ti_{70.5}Fe_{29.5}$ eutectic phase with interface spacing less than 1200 nm facilitates to enhance the scattering of phonons in the present case, most possibly similar to an earlier observation reported by Wu et al.[45] in Ag-Pb-Te materials. However, the exact mechanism of effective phonon scattering with long to short mean path to significantly reducing the thermal conductivity in such a complex lamellae eutectic incorporated in the large concentration of submicron grains of half-Heusler phase, is not clear at this stage and would require further study. The effective value of thermal conductivities of the HH TiNiSn/eutectic $Ti_{70.5}Fe_{29.5}$ composites were also calculated assuming TiNiSn as HH matrix and $Ti_{70.5}Fe_{29.5}$ eutectic as inclusion by using the effective medium theory in the light of Maxwell–Eucken (Eq. 2) approximations,[57]

$$K = \frac{k_1 v_1 + k_2 v_2 \frac{3k_1}{2k_1 + k_2}}{v_1 + v_2 \frac{3k_1}{2k_1 + k_2}} \quad \text{.....(2)}$$

Where K is the effective thermal conductivity of the composite, κ_1 = continuous phase i.e. the thermal conductivity of the matrix, κ_2= dispersed phase i.e. thermal conductivity of the inclusion, and v_1 and v_2 are the volume fractions of the matrix and second phase respectively. The value of κ_2 i.e. thermal conductivity of $Ti_{70.5}Fe_{29.5}$ eutectic inclusion was taken from the data shown in the inset of Fig. 5(a).

Based on the model described above, the calculated thermal conductivity of all the composites present similar trend with the experimentally observed thermal conductivities of the composites with slight variations in their values as shown by their corresponding line curves in Fig. 5(a). The slight deviation in the thermal conductivities may occur due to either the experimental error or approximation limit of the model.

The lattice thermal conductivity was obtained by subtracting the electronic thermal conductivity from the total measured thermal conductivity. The Wiedemann-Franz law has been used to calculate the electronic thermal conductivity ($\kappa_e = L\sigma T$, where L is Lorenz number, σ, the electrical conductivity and T, the temperature in K) which is shown in Fig. 5(b). Here, we use the temperature dependent Lorenz number calculated particularly for TiNiSn by Birkel et. al. [58] and the bipolar contribution was taken into account by assuming $\kappa_{lattice} \sim 1/T$[59] Figure 5(c) represents the temperature dependent lattice thermal conductivity. The lattice thermal conductivity of all the samples was observed to decrease with increasing temperature, showing similar falling trend in the total thermal conductivity. The lattice thermal conductivity of TiNiSn half-Heusler at room temperature is approximately 5.0 W/mK which agrees well with previously published results.[60] Thus, we notice that the lattice thermal conductivity significantly contributes to the total thermal conductivity as envisaged from Fig 5 (b) and Fig 5 (c). Interestingly, a drastic reduction in the lattice thermal conductivity in the composite with mass ration 33:1 was observed which is attributed to numerous lamellae interfaces in matrix to disrupt the heat carrying phonons to lowering the lattice thermal conductivity. The temperature dependent lattice thermal conductivity shows a remarkable decrease $\kappa_l \approx 0.3$ $Wm^{-1}K^{-1}$ at high temperature which is attributed to the short range phonon scattering due to lamellae structure at high temperature in the HH matrix. Thus such structural modification by incorporating the lamellae eutectic inclusions, leads to the reduced lattice thermal conductivity which is about more than 70% reduction when compared to the lattice thermal conductivity of TiNiSn which is best reported high ZT by Downie et. al.[28]

3.4 Thermoelectric figure of merit:

The temperature dependence of ZT of all the samples is calculated which is displayed in Fig 6. The ZT of the HH TiNiSn/eutectic $Ti_{70.5}Fe_{29.5}$ composites increases with rising temperature. The maximum ZT ≈ 0.41 at temperature of 773 K for HH TiNiSn/eutectic $Ti_{70.5}Fe_{29.5}$ composite was optimized for the mass ratio 33:1, which is significantly enhanced than ZT≈ 0.20 at 773 K for bare TiNiSn. Thus combining a large increase (~57 %) in the power factor due to significant enhancement of electrical conductivity (~115%), along with 25% reduction in the thermal conductivity, the ZT of the HH TiNiSn/eutectic $Ti_{70.5}Fe_{29.5}$ composite with mass ratio 33:1 was calculated to be about 105% larger than that of bare TiNiSn sample.

4. Conclusion and Future Prospects:

In Summary, novel half-Heusler (HH) TiNiSn/eutectic $Ti_{70.5}Fe_{29.5}$ composites have been fabricated by incorporating metallic $Ti_{70.5}Fe_{29.5}$ eutectic alloy in pre-synthesized TiNiSn (HH) precursors using high energy mechanical ball milling and further consolidated by spark plasma sintering. A significant enhancement in the electrical conductivity (~115% larger value than bare TiNiSn) with moderate decrease in the Seebeck coefficient results to a large increase power factor (~57% larger value than bare TiNiSn) of HH TiNiSn/eutectic $Ti_{70.5}Fe_{29.5}$ composite with mass ratio 33:1 was realized. Moreover, despite the metallic nature of lamellae eutectic $Ti_{70.5}Fe_{29.5,}$ the thermal conductivity of this composite was also significantly decreased (~25% reduced value than bare TiNiSn)). The drastic reduction in the thermal conductivity is accounted due to significant reduction in the lattice thermal conductivity due to effective phonon scattering due to submicron lamellae β-Ti and TiFe interfaces of $Ti_{70.5}Fe_{29.5}$ eutectic phase and due to numerous grain boundaries. A higher ZT of 0.41 at 773 K was obtained in the HH TiNiSn/eutectic $Ti_{70.5}Fe_{29.5}$ composite (mass ratio::33: 1) which is 105 % larger than that of normal TiNiSn half-Heusler. Such a significant increase in ZT is quite remarkable considering that only a small amount of $Ti_{70.5}Fe_{29.5}$ was introduced to form such an efficient composite. Relatively, earth abundance and non-toxicity of Ti, Ni, Sn and Fe involved in such a composite materials make them a cheap, alternative option and finds widespread use over high scarcity and price of Te, Pb used in the commercialized state-of-the-art thermoelectric materials. We strongly believe that the present strategy of fabricating such composite by incorporating submicron

metallic lamellae eutectic in the TiNiSn half-Heusler may be very effective and promising approach and can be deployed not to only TiNiSn half-Heusler but to the most of the existing potential bulk thermoelectric materials to enhance the thermoelectric performance.

Acknowledgement

This work was supported by CSIR-TAPSUN (NWP- 54) programme entitled "Novel approaches for solar energy conversion under technologies and products for solar energy utilization through networking." The authors thank Prof. R. C. Budhani (Director, CSIR-NPL), Dr. A. M. Biradar (CSIR-NPL) and Dr. Jiji Pullikotil (CSIR-NPL) for their continuous encouragement. We acknowledge Dr. Sunil Pandey (NIMS University, Jaipur) for providing the room temperature Hall data. One of the authors AB greatly acknowledges UGC-CSIR for financial support. The technical support rendered by Dr. Ajay Dhar, Mr. Radhey Shyam, and Mr. Naval Kishor Upadhyay is gratefully acknowledged**.**

References:

1. G. J. Snyder and E. S. Toberer, Nat. Mater., 2008, **7**, 105.
2. (a) B. Poudel, Q. Hao, Y. Ma, Y. Lan, A. Minnich, B. Yu, X. Yan, D. Wang, A. Muto, D. Vashaee, X. Chen, J. Liu, M. S. Dresselhaus, G. Chen and Z. Ren, *Science*, 2008, **320**, 634. (b) S. Yu, J. Yang, Y. Wu, Z. Han, J. Lu, Y. Xie and Y. Qian, *J. Mater. Chem.*, 1998, **8**, 1949. (c) J. Shen, T. Zhu, X. Zhao, S. Zhang, S. Yanga and Z. Yina, *Energy Environ. Sci.*, 2010, **3**, 1519. (d) M. E. Anderson, S. S. N. Bharadwaya and R. E. Schaak, *J. Mater. Chem.*, 2010, **20**, 8362. (e) S. Sumithra, N. J. Takas, D. K. Misra, W. M. Nolting, P. F. P. Poudeu and K. L. Stokes, *Adv. Energy Mater.*, 2011, **1**, 1141.
3. K. F. Hsu, S. Loo, F. Guo, W. Chen, J. S. Dyck, C. Uher, T. Hogan, E. K. Polychroniadis and M. G. Kanatzidis, *Science*, 2004, **303**, 818.

4. J. Androulakis, K. F. Hsu, R. Pcionek, H. Kong, C. Uher, J. J. D'Angelo, A. Downey, T. Hogan and M. G. Kanatzidis, *Adv. Mater.*, 2006, **18**, 1170.

5. (a) J. R. Sootsman, H. Kong, C. Uher, J. J. D'Angelo, C. I. Wu, T. P. Hogan, T. Caillat and M. G. Kanatzidis, Angew. Chem., *Int. Ed.*, 2008, **47**, 8618. (b) K. Ahn, K. Biswas, J. He, I. Chung, V. Dravid and M. G. Kanatzidis, *Energy Environ. Sci.***,** 2013, **6**, 1529.

6. R. Basu, S. Bhattacharya, R. Bhatt, M. Roy, S. Ahmad, A. Singh, M. Navaneethan, Y. Hayakawa, D. K. Aswal and S. K. Gupta, *J. Mater. Chem. A*, 2014, **2**, 6922.

7. (a) G. Rogl A. Grytsiv P. Rogl E. Bauer M. Hochenhofer E. Schafler ,Acta Materialia DOI: 10.1016/j.actamat.2014.05.051 (b) B. C. Sales, D. Mandrus, R. K. Williams, *Science,* 1996, **272**, 1325. (c) R. C. Mallik, R. Anbalagan, G. Rogl, E. Royanian, P. Heinrich, E. Bauer, P. Rogl and S. Suwas, *Acta Materialia*, 2013, **61**, 6698–6711. (d) R. C. Mallik, R. Anbalagan, K. K. Raut, A. Bali, E. Royanian, E. Bauer, G. Rogl, P. Rogl, *Journal of Physics: Condensed Matter*, 2013, **25**, 105701. (d) E. Bauer, St. Berger, Ch. Paul, M. Della Mea, G. Hilscher, H. Michor, M. Reissner, W. Steiner, A. Grytsiv, P. Rogl, and E. W. Scheidt, *Phys. Rev. B,* 2002, **66**, 214421. (e) L Zhang, A Grytsiv, P Rogl, E Bauer and M Zehetbauer, *J. Phys. D: Appl. Phys.*, 2009, **42,** 225405. (f) A. Grytsiv, P. Rogl, St. Berger, Ch. Paul, E. Bauer, C. Godart, B. Ni, M. M. Abd-Elmeguid, A. Saccone, R. Ferro, and D. Kaczorowski, *Phys. Rev. B,* 2002, **66**, 094411. (g) J. W. Graff, X. Zeng, A. M. Dehkordi, J. He and T. M. Tritt, *J. Mater. Chem. A*, 2014, **2**, 8933-8940. (h) G. Rogl, A. Grytsiv, P. Rogl, N. Peranio, E. Bauer, M. Zehetbauer, O. Eibl, *Acta Materialia*, 2014, **63**, 30–43.

8. (a) A. Bhardwaj and D. K. Misra, *RSC Adv.*, 2014, **4**, 34552. (b) G. J. Snyder, M. Christensen, E. Nishibori, T. Caillat and B. B. Iversen, *Nature Mater.*, 2004, **3**, 458. (c) S. R.

Brown, S. M. Kauzlarich, F. Gascoin and G. J. Snyder, *Chem. Mater.*, 2006, **18**, 1873. (d) A. Bhardwaj, A. Rajput, A. K. Shukla, J. J. Pulikkotil, A. K. Srivastava, A. Dhar, G. Gupta, S. Auluck, D. K. Misra and R. C. Budhani, *RSC Adv.*, 2013, **3**, 8504. (e) S. K. Bux, A. Zevalkink, O. Janka, D. Uhl, S. Kauzlarich, J. G. Snyder and J. P. Fleurial, *J. Mater. Chem. A*, 2014, **2**, 215. (f) N. Kazem, W. Xie, S. Ohno, A. Zevalkink, G. J. Miller, G. J. Snyder, and S. M. Kauzlarich, *Chem. Mater.* 2014, **26**, 1393. (g) A. Zevalkink, Y. Takagiwa, K. Kitahara, K. Kimura and G. J. Snyder *Dalton Trans.*, 2014, **43**, 4720.

9. (a) S. Chen and Z. F. Ren, *Materials Today*, 2013, **16**, 387. (b) W. Xie, A. Weidenkaff, X. F. Tang, Qi. Zhang, S. J. Poon and T. M. Tritt, Nanomaterials 2012, **2**, 379. (c) J. W. G. Bos and R. A. Downie*, J. Phys.: Condens. Matter*, 2014, 26, 433201.(d) S. J. Poon, D. Wu, S. Zhu, W. Xie, T. M. Tritt, P. Thomas and R. Venkatasubramanian, *J.of Mat. Res*, 2011, 26 2795.

10. (a) X. Yan, G. Joshi, W. S. Liu, Y. C. Lan, H. Wang, S. Lee, J. W. Simonson, S. J. Poon, T. M. Tritt, G. Chen and Z. F. Ren, *Nano Lett.* 2011, **11**, 556. (b) E. Rausch, B. Balke, S. Ouardi and C. Felser, *Phys. Chem. Chem. Phys.,*2014, DOI: 10.1039/c4cp02561j (c) X. Yan, W. Liu, S. Chen, H. Wang, Q. Zhang, G. Chen and Z. F. Ren, *Adv. Energy Mater.*, 2013, **3** 1195. (d) C. Fu, T. J. Zhu, Y. Pei, H. Xie, H. Wang, G. J. Snyder, Y. Liu, Y. Liu and X. B. Zhao, *Advanced Energy Materials*, 2014 DOI: 10.1002/aenm.201400600 (e) T. Wu, W. Jiang, X. Li, Y. Zhou and L. D. Chen *J. Appl. Phys.*, 2007, **102**, 103705. (f) X. Yan, W. Liu, H. Wang, S. Chen, J. Shiomi, K. Esfarjani, H. Wang, D. Wang, G. Chen and Z. Ren, *Energy Environ. Sci.*, 2012, **5**, 7543.

11. (a) S. Sakurada, N. Shutoh, *Appl. Phys. Lett.* 2005, **86**, 082105. (b) D. K. Misra, A. Bhardwaj and S. Singh, *J. Mater. Chem. A*, 2014, **2**, 11913- 11921. (c) G. Joshi, X. Yan, H. Wang, W.

Liu, G. Chen, Z. F. Ren, *Adv. Energy Mater.* 2011, **1**, 643. (d) S. R. Culp, S. J. Poon, N. Hickman, T. M. Tritt, and J. Blumm, *Appl. Phys. Lett.*, 2006, **88**, 042106. (e) A. Bhardwaj, D. K. Misra, J. J. Pulikkotil, S. Auluck, A. Dhar and R. C. Budhani, *Appl. Phys. Lett.*, 2012, 101, 133103. (f) C. Yu, T. J. Zhu, R. Z. Shi, Y. Zhang, X. B. Zhao and J. He, *Acta Mater.*, 2009, **57**, 2757. (g) Q. Shen, L. Chen, T. Goto, T. Hirai, J. Yang, G. P. Meisner, C. Uher, *Appl. Phys. Lett.*, 2001, **79**, 4165

12. J. Pierre, R. V. Skolozdra, J. Tobola, S. Kaprzyk, C. Hordequin, M. A. Kouacou, I. Karla, R. Currat and E. Lelievre-Berna, *J. Alloys Compd.*, 1997, **262**, 101–107.
13. J. Tobola and J. Pierre, *J. Alloys Compd.*, 2000, **296**, 243–252.
14. S. W. Kim, Y. Kimura, Y. Mishima, *Intermetallics*, 2007, **15**, 349–356.
15. E. Quarez, K.-F. Hsu, R. Pcionek, N. Frangis, E. K. Polychroniadis, and M. G. Kanatzidis, *J. Am. Chem. Soc.*,2005, **127**, 9177.
16. P. F. P. Poudeu, J. D'Angelo, H. J. Kong, A. Downey, J. L. Short, R. Pcionek, T. P. Hogan, C. Uher, and M. G. Kanatzidis, *J. Am. Chem. Soc.*, 2006, **128**, 14347.
17. P. F. P. Poudeu, J. D'Angelo, A. D. Downey, J. L. Short, T. P. Hogan, and M. G. Kanatzidis, *Angew. Chem., Int. Ed.*, 2006, **45**, 3835.
18. J. Androulakis, K. F. Hsu, R. Pcionek, H. Kong, C. Uher, J. J. Dangelo, A. Downey, T. Hogan, and M. G. Kanatzidis, *Adv. Mater.*, 2006, **18**, 1170.
19. J. R. Sootsman, R. J. Pcionek, H. J. Kong, C. Uher, and M. G. Kanatzidis, *Chem. Mater.*, 2006, **18**, 4993.
20. A. F. Ioffe, *Semiconductor Thermoelements and Thermoelectric Cooling*_Infosearch, London, 1957.
21. M. G. Kanatzidis, *Acc. Chem. Res.*,2005, **38**, 359.

22. G. S. Nolas, J. Poon, and M. Kanatzidis, MRS Bull., 2006, **31**,199.

23. W. Kim, J. Zide, A. Gossard, D. Klenov, S. Stemmer, A. Shakouri, and A. Majumdar, *Phys. Rev. Lett.*, 2006, **96**, 045901.

24. D. Li, S. T. Huxtable, A. R. Abramson, and A. Majumdar, *J. Heat Transfer*, 2005, **127**, 108.

25. A. Majumdar, *Science*, 2004, **303**, 777.

26. L. D. Hicks and M. S. Dresselhaus, *Phys. Rev. B*, 1993, **47**, 12727.

27. R. A. Downie, D. A. MacLaren and J.-W. G. Bos, *J. Mater. Chem. A*, 2014, **2**, 6107.

28. R. A. Downie, D. A. MacLaren, R. I. Smith and J.-W. G. Bos, Chem. Commun., 2013, **49**, 4184.

29. X. Y. Huang, Z. Xu, L. D. Chen, *Solid State Commun.*, 2004, **130**, 181.

30. L. D. Chen, X. Y. Huang, M. Zhou, X. Shi, W. B. Zhang, *J. Appl. Phys.*, 2006, **99**, 064305.

31. S. J. Poon, D. Wu, S. Zhu, W. Xie, T. M. Tritt, P. Thomas, R. Venkatasubramanian, *J. Mater. Res.*, 2011, **26**, 2795.

32. X. Y. Huang, Z. Xu, L. D. Chen, X. F. Tang, *Key Eng. Mater.*, 2003, **249**, 79.

33. D. K. Misra, J. P. A. Makongo, P. Sahoo, M. R. Shabetai, P. Paudel, K. L. Stokes, P. F. P. Poudeu, *Sci. Adv. Mater.* 2011, **3**, 607.

34. X. Y. Huang, L. D. Chen, X. Shi, M. Zhou, Z. Xu, *Key Eng. Mater*. 2005, **280**, 385.

35. R. Yaqub, P. Sahoo, J. P. A. Makongo, N. Takas, P. F. P. Poudeu, K. L. Stokes, *Sci. Adv. Mater.* 2011, **3**, 633.

36. D. K. Misra, J. P. A. Makongo, M. R. Shabetai, G. S. Chaubey, J. Wiley, K. L. Stokes, P. F. P. Poudeu, 2010 MRS Spring Meeting. 1267, 1267-DD06-12

37. J. R. Sootsman, J. He, V. P. Dravid, S. Ballikaya, D. Vermeulen, C. Uher, and M. G. Kanatzidis, Chem. Mater. 2010, **22**, 869–875 869

38. J.Q. He, A. Gueguen, J.R. Sootsman, J.C. Zheng, L. J. Wu, Y.M. Zhu, M.G. Kanatzidis, V.P. Dravid *Journal of the American Chemical Society,* 2009, **131,** 17828

39. J.R. Sootsman, J.Q. He, V.P. Dravid, C.P. Li, C. Uher, M.G. Kanatzidis *J. App. Phy.,* 2009, **105**, 083718.

40. T. Ikeda, L. A. Collins, V. A. Ravi, F. S. Gascoin, S. M. Haile, and G. J. Snyder, *Chem. Mater.*, 2007, **19**, 763.

41. S.N. Girard, J. He, X.Y. Zhou, D. Shoemaker, C.M. Jaworski, C. Uher, V.P. Dravid, J.P. Heremans and M.G. Kanatzidis, *JACS,* 2011, **133**, 16588.

42. K. W. Jang, D. H. Lee, Fourteenth International Conference on Thermoelectrics, 108 (IEEE, 1995).

43. T. Ikeda, S. M. Haile, V. A. Ravi, H. Azizgolshani, F. Gascoin, G. J. Snyder, *Acta Mater.*, 2007, **55**, 1227.

44. W. K. Liebmann,and E. A. Miller, *J. Appl. Phys.*, 1963, **34,** 2653.

45. H. J. Wu, W. J. Foo, S. W. Chen, and G. J. Snyder, *Appl. Phys. Lett.,* 2012, **101**, 023107.

46. G. I. Isakov, *Semiconductors*, 2005, **39**, 738.

47. G. I. Isakov, *J. Eng. Phys. Thermophys,* 2004, **77**, 1062.

48. I. V. Dement'ev and V. V. Leonov, *Inorg. Mater.* 1988, **24**, 19.

49. V. V. Leonov and Z. K. Gantimurova, *Inorg. Mater.,* 1987 **23**, 1683.

50. V. V. Leonov and Y. E. Spektor, *Inorg. Mater.*, 1980, **16**, 918.

51. V. V. Leonov, *Inorg. Mater.,* 1985, **21**, 265.

52. C. Leyens, M. Peters, *Titanium and titanium alloys: fundamentals and applications*, vol. 1. Weinheim: Wiley-VCH, 2003.

53. D. K. Misra, R. K. Rakshit, M. Singh, P. K. Shukla, K. M. Chaturvedi, B. Sivaiah, B. Gahtori, A. Dhar, S. W. Sohn, W. T. Kim, D. H. Kim, *Materials & Design*, 2014, **58**, 551.
54. D.K. Misra, S.W. Sohn, H. Gabrisch, W.T. Kim, D.H. Kim, High strength Ti–Fe–(In, Nb) composites with improved plasticity, *Intermetallics*, 2010, **18**, 342.
55. D. Keazler, D. Cahen, J. Lbers *POLSQ FORTRAN program*, IL: Northwestern University Evanston, 1984.
56. V. Johnson and K. Lark-Horovitz, *Phys. Rev.*, 1953, **92**, 226
57. J. Wang, J. K. Carson, M. F. North, and D. J. Cleland, *Int. J. Heat Mass Transfer*, 2008, **51**, 2389
58. C. S. Birkel, J. E. Douglas, B. R. Lettiere, G. Seward, N. Verma, Y. Zhang, T. M. Pollock, R. Seshadri and G. D. Stucky, *Phys. Chem. Chem. Phys.*, 2013,**15**, 6990.
59. H. Kitagawa, M. Wakatsuki, H. Nagaoka, H. Noguchi, Y. Isoda, K. Hasezaki, and Y. J. Noda, *Phys. Chem. Solids*, 2005, **66**, 1635.
60. C. S. Birkel, W. G. Zeier, J. E. Douglas, B. R. Lettiere, C. E. Mills, G. Seward, A. Birkel, M. L. Snedaker, Y. Zhang, G. J. Snyder, T. M. Pollock, R. Seshadri and G. D. Stucky, Chem. Mater., 2012, 24, 2558–2565.

Figure Caption:

Figure 1. a) X-ray diffraction (XRD) pattern of TiNiSn HH and its JCPDS card no. 00-023-1281. The ball and stick arrangement for half-Heusler (HH) structure illustrating the atomic arrangement is shown in inset of Fig. 1(a).

b) XRD pattern of $Ti_{70.5}Fe_{29.5}$ eutectic phase and HH TiNiSn/eutectic $Ti_{70.5}Fe_{29.5}$ composites with mass ratio of 33:1.

Figure 2. FE-SEM micrographs of a) TiNiSn parent compound showing a single phase contrast of half-Heusler phase, b) EDAX spectrum of TiNiSn shows qualitatively the presence of constituent elements Ti, Ni and Sn and the composition analysis confirms the composition to be very close to TiNiSn, c) SEM image of $Ti_{70.5}Fe_{29.5}$ eutectic phase showing alternating bright and dark phase contrasts which are more clearly visible in the inset of Fig 2 (c), d) EDAX spectrums obtained from these alternating lamellae as marked in Fig 2(c) confirms the presence of β-Ti and TiFe phases of eutectic $Ti_{70.5}Fe_{29.5}$ alloy, e) SEM morphology of HH TiNiSn/eutectic $Ti_{70.5}Fe_{29.5}$ composite with mass ratio of 33:1 reveals the two phase contrast mixture, g) magnified image of HH TiNiSn/eutectic $Ti_{70.5}Fe_{29.5}$ composite showing a clear eutectic feature in HH matrix. The composition of eutectic alloy was confirmed by EDAX analysis.

Figure 3. a) TEM image obtained from the specimen of TiNiSn presents highly densified grains, b) SAED pattern corresponding to the TiNiSn HH phase with zone axis [1 -1 1], c) TEM image of HH TiNiSn/eutectic $Ti_{70.5}Fe_{29.5}$ composite with mass ratio of 33:1 showing two phase contrasts, one with eutectic feature (marked be dotted area) and HH as matrix phase. The relatively better clarity of the eutectic feature is presented in the inset of Fig. 3(c), d) The SAED pattern taken from the eutectic feature confirms the β-Ti and TiFe of eutectic phase.

Figure 4: a) Temperature dependence of the electrical conductivity σ (T), b) temperature dependence of the Seebeck coefficient, α (T), c) temperature dependent power Factor, $\sigma\alpha^2$(T) of bare TiNiSn (HH) and HH TiNiSn/eutectic $Ti_{70.5}Fe_{29.5}$ composites with different mass ratios of 100:1, 33:1 and 20:1.

Figure 5: a) Temperature dependence behavior of the total thermal conductivity κ (T) of bare TiNiSn (HH) and HH TiNiSn/eutectic $Ti_{70.5}Fe_{29.5}$ composites with different mass ratios of 100:1, 33:1 and 20:1 with calculated effective thermal conductivity for all the composites by using the effective medium theory and Maxwell–Eucken approximations and inset of fig 5 (a) shows the total thermal conductivity of eutectic $Ti_{70.5}Fe_{29.5}$, b) electronic and c) lattice thermal conductivity of bare TiNiSn (HH) and HH TiNiSn/eutectic $Ti_{70.5}Fe_{29.5}$ composites with different mass ratios of 100:1, 33:1 and 20:1.

Figure 6: Temperature dependence of thermoelectric figure of merit of bare TiNiSn (HH) and HH TiNiSn/eutectic $Ti_{70.5}Fe_{29.5}$ composites with different mass ratios of 100:1, 33:1 and 20:1.

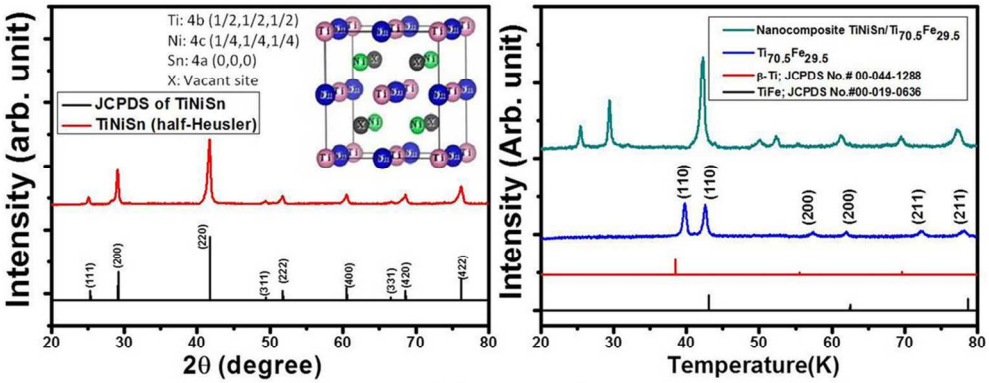

Figure 1

102x45mm (300 x 300 DPI)

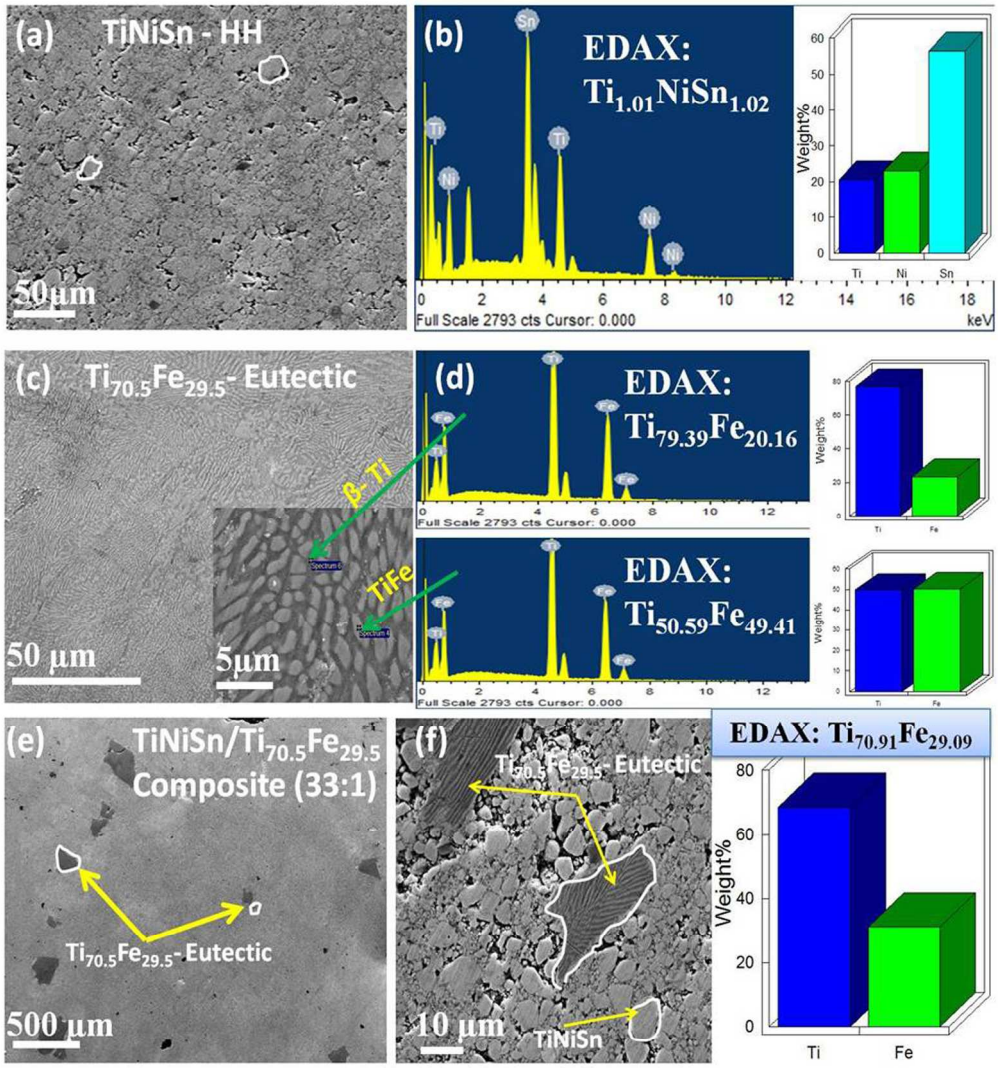

Figure 2

189x217mm (300 x 300 DPI)

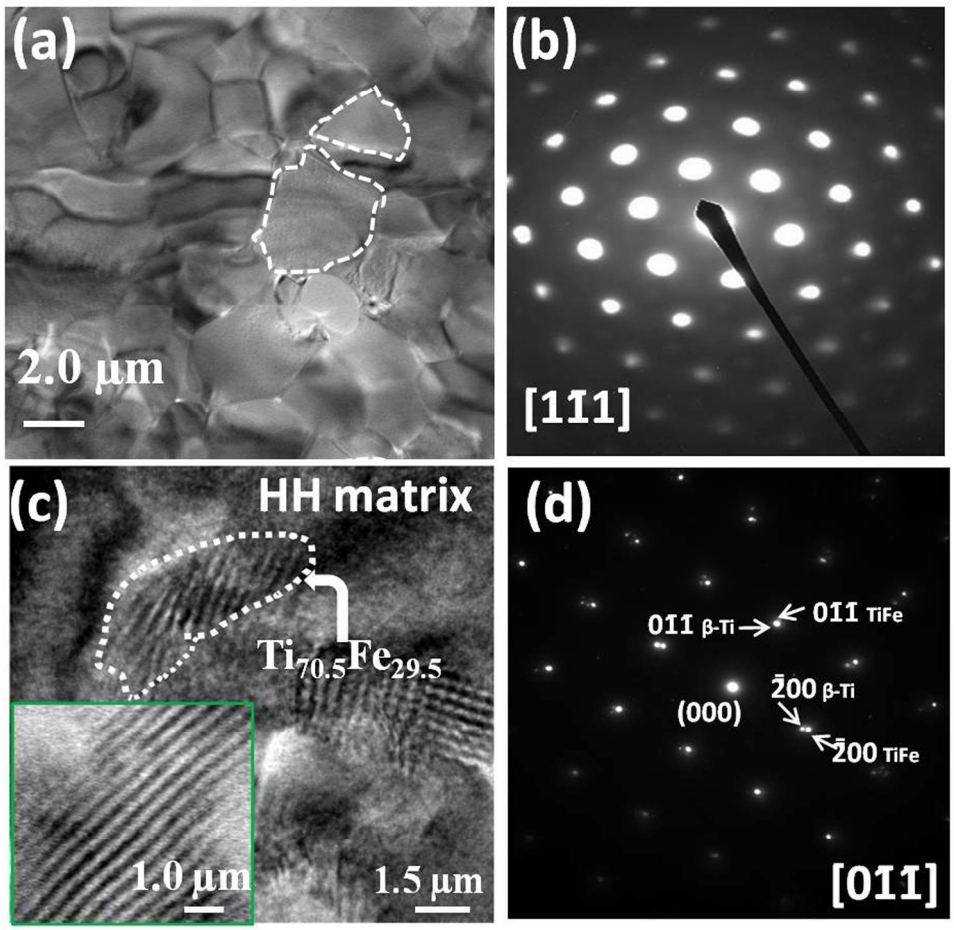

Figure 3

175x187mm (300 x 300 DPI)

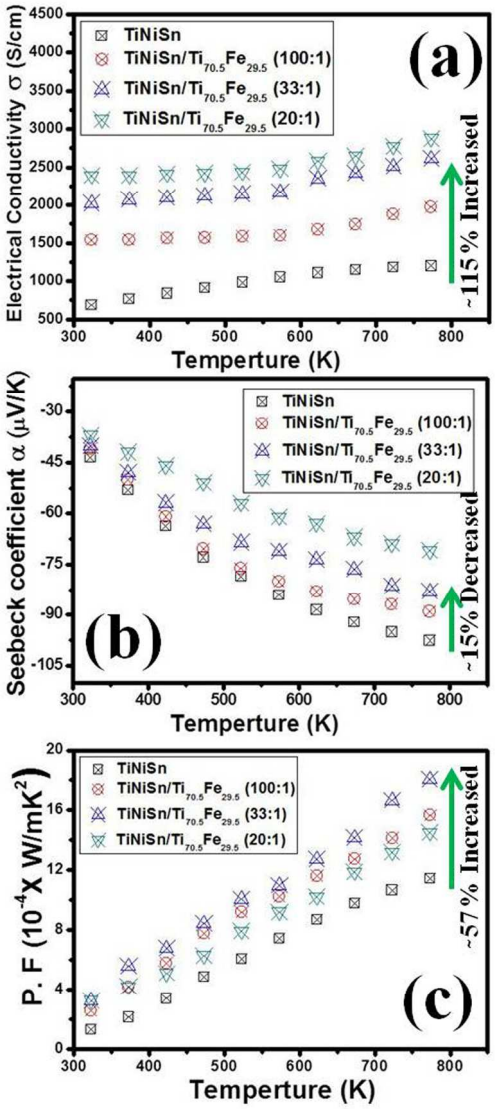

Figure 4

197x454mm (300 x 300 DPI)

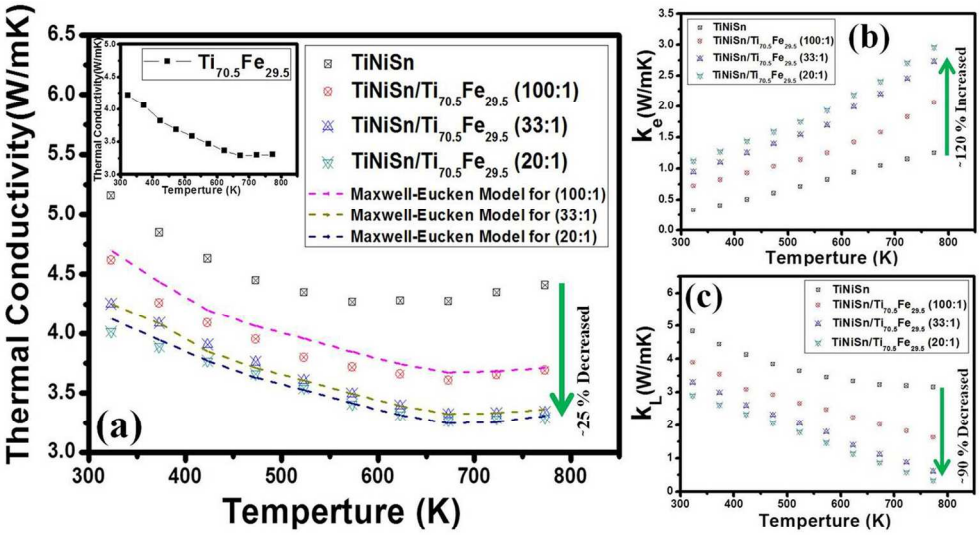

Figure 5

162x103mm (300 x 300 DPI)

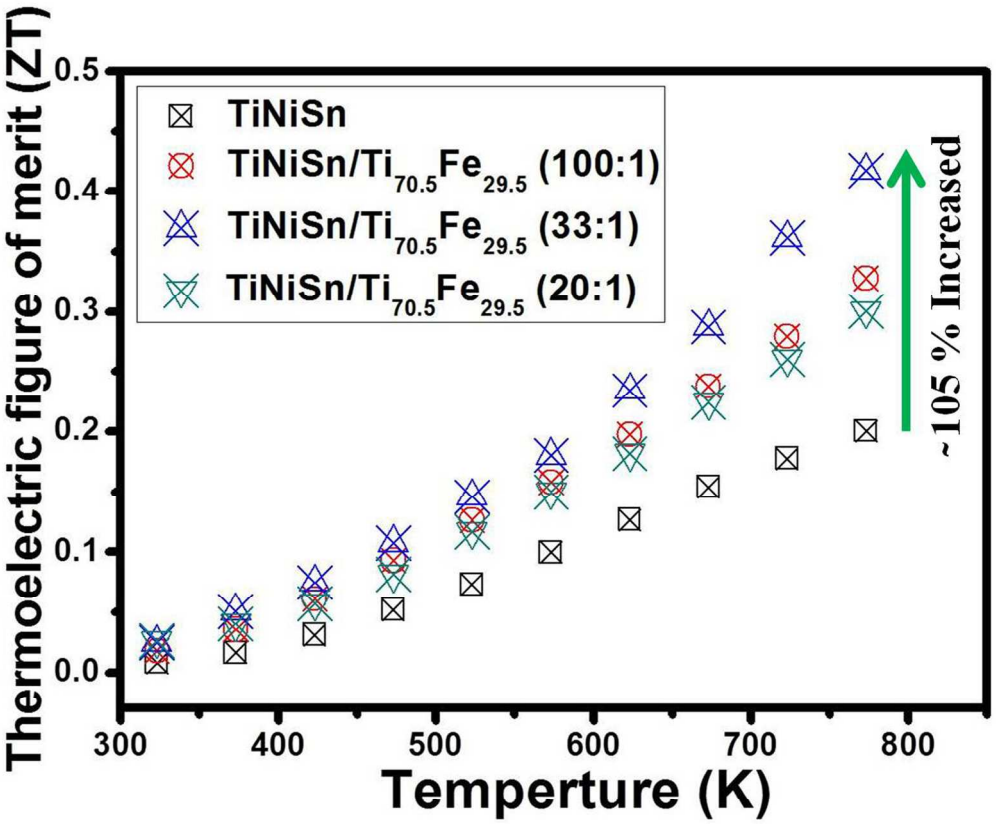

Figure 6

177x160mm (300 x 300 DPI)

Nominal Composition	Hall Coefficient (R_H) × 10^{-2} cm^3C^{-1}	Carrier conc. n (10^{19} cm^{-3})	Mobility μ ($cm^2V^{-1}s^{-1}$)
TiNiSn	10.5	5.9	121
TiNiSn/$Ti_{-0.5}Fe_{29.5}$(100:1)	6.7	9.3	127
TiNiSn/$Ti_{-0.5}Fe_{29.5}$(33:1)	6.3	9.8	159
TiNiSn/$Ti_{-0.5}Fe_{29.5}$(20:1)	5.8	10.3	167

Table 1. Hall measurement data of half-Heusler (HH) TiNiSn/eutectic $Ti_{-0.5}Fe_{29.5}$ nanocomposites at room temperature

63x16mm (300 x 300 DPI)